RESEARCH ARTICLE | MAY 16 2025

Characterization of negative differential resistance in asymmetric nanopores obtained from two soluble electrolytes

Patricio Ramirez ; Sergio Portillo ; Salvador Mafe ; Zuzanna S. Siwy ; Javier Cervera

J. Chem. Phys. 162, 194707 (2025)
https://doi.org/10.1063/5.0255394
CHORUS

The Journal of Chemical Physics ARTICLE pubs.aip.org/aip/jcp

Characterization of negative differential resistance in asymmetric nanopores obtained from two soluble electrolytes

Cite as: J. Chem. Phys. 162, 194707 (2025); doi: 10.1063/5.0255394
Submitted: 29 December 2024 • Accepted: 3 April 2025 •
Published Online: 16 May 2025

Patricio Ramirez,[1] Sergio Portillo,[2] Salvador Mafe,[2] Zuzanna S. Siwy,[3] and Javier Cervera[2,a)]

AFFILIATIONS

[1] Departament de Física Aplicada, Universitat Politècnica de València, E-46022 Valencia, Spain
[2] Departament de Física de la Terra i Termodinàmica, Universitat de València, E-46100 Burjassot, Spain
[3] Department of Physics and Astronomy, University of California, Irvine, California 92697, USA

[a)] **Author to whom correspondence should be addressed:** jcervera@uv.es

ABSTRACT

Negative differential resistance (NDR) phenomena in nanofluidic diodes are characterized by a decrease in the electrical current with the increase in the transmembrane potential beyond a system-dependent threshold voltage. Here, we describe the NDR due to a nanoscale salt precipitation that occurs in a conical nanopore in contact with two highly soluble salts in the external solutions. The new experimental design permits tunable and reproducible NDR effects that can be characterized from the I–V curves for different pairs of soluble salts reacting at the pore tip to form the salt precipitate. The effects of pH and salt concentration on the precipitation, together with the use of electrolytes with different temperature-dependent solubilities, provide a complete description of the chemical NDR mechanism. In addition, the good reproducibility and stability observed over different voltage cycles suggest that the threshold potential needed for precipitation can be used for Ca^{2+} sensing in the range 1–1000 mM.

I. INTRODUCTION

Negative differential resistance (NDR) phenomena are characterized by a decrease in the electrical current with the increase in the transmembrane potential, V, beyond a threshold voltage, V_{th}, whose magnitude is system dependent. It has been described in electronic solid-state junctions[1] and, more recently, in ionic liquid-state nanopores and membranes.[2–10] Ionic NDR has been observed in a wide variety of systems related to elastomeric effects,[2] divalent cation-gating and oscillatory phenomena,[3] pressure-induced ionic flows,[4] electrically modulated ionic conduction,[5,6] water and ionic-liquid mixtures,[7] pH-modulated transport,[8] KF solutions at low concentration,[9,10] and salt precipitation phenomena with multivalent and monovalent salts.[11–14]

NDR is typically probed through recording current–voltage curves. It is a robust property that has been reported in a range of nanopore systems and experimental conditions, where reproducible switching between high and low conductance states at the threshold voltage was observed.[9,10,12–14] The high sensitivity of the transmembrane current to even small changes in voltage around V_{th} suggests the possibility of applying nanopores that exhibit NDR to amplify weak electrical perturbations, e.g., in nanofluidic sensing and actuation.[15–17] In addition, the hysteresis effects observed in current–voltage curves under particular experimental conditions suggest further applications in static and oscillatory memories, memristive devices, neuromorphic computing, and hybrid circuits.[17–25]

Here, we provide new physico-chemical insights of the NDR phenomena associated with the nanoscale precipitation that occurs at the tip of single negatively charged nanopores fabricated in polymeric foils. In order to limit the precipitation formation to a well-defined region inside a nanopore, a pore was placed in a conductivity cell whose chambers were filled with different highly soluble salts such that each salt contained either cations or anions creating the precipitate. Consequently, the precipitation formation was restricted to the pore volume where concentrations of both ions,

sourced from opposite pore openings, were enhanced. We present a general procedure that results in I–V curves showing reproducible NDR phenomena from a series of soluble salts reacting in the pore volume at the pore tip region and forming the precipitate. In addition, we describe the pH and salt concentration effects on the precipitation and consider electrolytes with different temperature-dependent solubilities. The stability and reproducibility of the threshold potential V_{th} needed for precipitation, over multiple repeated different cycles, allow us to define a calibration curve for Ca^{2+} sensing in the range 1–1000 mM. Salt solubility phenomena are of interest to biophysical chemistry, chemical engineering, and pharmaceutical sciences. Here, we have emphasized the case of calcium ions in nanoscale geometries.

II. EXPERIMENTAL

The polymeric samples with single conical nanopores have been prepared as described previously.[26,27] The approximately conical pores are obtained by the track-etching technique that begins with irradiating a 12.5 μm thick polyimide foil by single swift heavy ions (Au or U ions at the Helmholtzzentrum für Schwerionenforschung, Darmstadt, Germany). The resulting tracks are developed by wet chemical etching in sodium hypochlorite, which leads to the formation of carboxyl groups on the pore walls and membrane surface. Consequently, the pores are negatively charged in neutral and basic solutions.[24,26] The pores used in this study had tip and base radii in the range 4–30 and 320–480 nm, respectively, as obtained by imaging the pore base using scanning electron microscopy and fitting the nanopore I–V curves in 100 mM KCl.[20] More details about the pore characteristics are given in Table S1 of the supplementary material. The I–V curves are measured employing a home-made electrochemical cell with Ag|AgCl electrodes connected to a potentiostat (BioLogic SP-200). The curves are recorded using a minimum of three cycles of triangular potential waves at scanning rates between 200 and 500 mV/s, depending on the amplitude of the wave. The experimental points are presented as measured, without averaging values in successive cycles. The cell is mounted on an anti-vibration table (Technical Manufacturing Corporation, Peabody, MA) and located within a double-shielded Faraday cage (Amuneal Manufacturing, Philadelphia, PA) to eliminate mechanical and electrical perturbations, respectively. The membrane exposed area is 1 cm^2. Different membrane samples have been employed for the sake of reproducibility.

III. RESULTS AND DISCUSSION

Figure 1 explains the mechanism of salt precipitation that occurs at a well-defined location along the pore axis. A single conically shaped nanopore is placed between two soluble salts, each containing a cation or anion that together form a weakly soluble salt in the pore volume. In our experiments, we used a wide range of salts that create precipitates with different solubilities, as

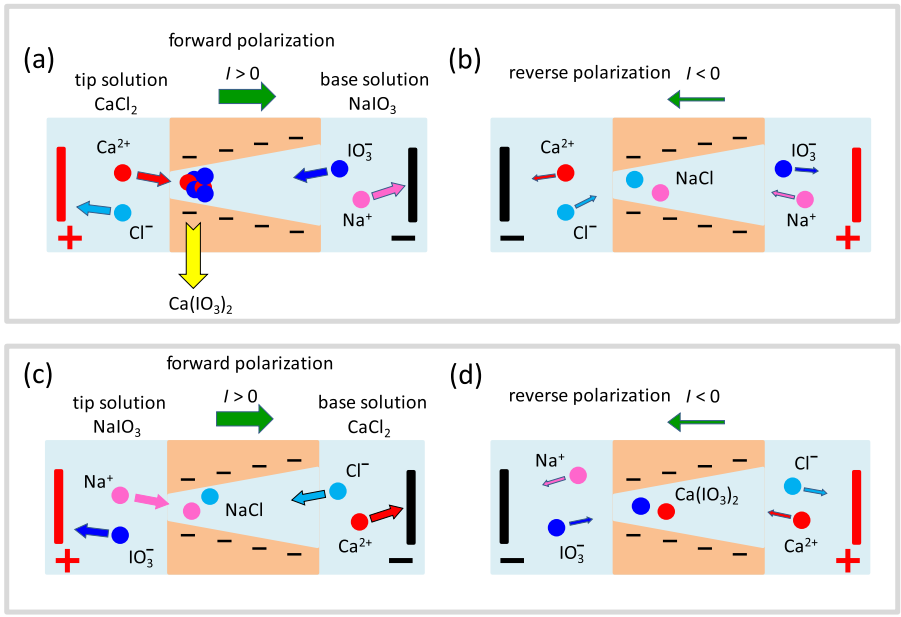

FIG. 1. Scheme of the nanoscale precipitation process that occurs at the negatively-charged pore tip. Note that the two electrolytes in the external solutions are soluble and show no precipitation in the bulk at the concentrations used here. (a) $CaCl_2$ (pore tip) and $NaIO_3$ (pore base) for $V > 0$. The cation Ca^{2+} and the anion IO_3^- accumulate at the tip pore. The resulting low solubility electrolyte $Ca(IO_3)_2$ precipitates at a threshold voltage V_{th}, thus blocking the pore and inducing the NDR reflected in the I–V curve. (b) For $V < 0$, the current drives the cation Na^+ and the anion Cl^- to the pore tip, thus forming the high solubility electrolyte NaCl. (c) $NaIO_3$ (pore tip) and $CaCl_2$ (pore base) also give NaCl at the pore tip for $V > 0$, and thus, no precipitation occurs. (d) On the contrary, $Ca(IO_3)_2$ is formed at the pore tip for $V < 0$. In this case, however, the negative pore charges do not allow a high enough IO_3^- flux, and thus, the ionic accumulation is not sufficient to reach the minimum electrolyte concentration needed for precipitation.[27,28]

listed in Table I. Figure 1 explains our setup with $CaCl_2$ placed at the pore tip and $NaIO_3$ at the pore base, as an electrolyte pair that can create the weakly soluble $Ca(IO_3)_2$. Due to the ion current rectification that conical pores exhibit, applying a forward voltage $V > 0$ leads to accumulation of both the cation Ca^{2+} and the anion IO_3^- at the pore tip [Fig. 1(a)]. When the positive voltage reaches a given threshold value V_{th}, the local concentrations of these ions exceed the solubility of $Ca(IO_3)_2$, and precipitates are formed. This is observed in the I–V curve as a negative differential resistance (NDR) leading to a step reduction in the current. At reverse voltage $V < 0$, on the other hand, the current drives the cation Na^+ and the anion Cl^- to the pore tip, thus forming the high solubility electrolyte NaCl in this case [Fig. 1(b)], and consequently, no NDR is observed. When the position of the reacting electrolytes is interchanged, as shown in Figs. 1(c) and 1(d), the high solubility electrolyte NaCl accumulates at the pore tip for $V > 0$ [Fig. 1(c)], yielding no NDR. At $V < 0$, even though Ca^{2+} and IO_3^- ions are driven into the pore [Fig. 1(d)], no precipitation or current blockage is observed because this voltage polarity causes ionic depletion in the pore, such that the ionic concentrations do not exceed the solubility of $Ca(IO_3)_2$.[27,28]

Using the experimental setup of Fig. 1, we have observed NDR in conical nanopores for different combinations of salts listed in Table I. In all cases, we used different salts on both sides of the membrane such that precipitates could form only in the pore volume. This is in contrast to previous studies that utilized mostly symmetric salt conditions on both sides of the membrane.[11–13] Our methodology shown here has several advantages. First, the weakly soluble salts are formed at the pore region close to the tip where the concentration of cations and anions, sourced from the opposite pore openings, is sufficiently high to exceed the solubility of the salt. The location of the precipitates is therefore very well defined. Second, the asymmetric salt arrangement facilitates probing precipitation in a broad range of electrolytes and concentrations, allowing multiple salt combinations, as shown in Table I. Indeed, as described below, the precipitates listed in Table I and formed inside a conical nanopore will induce distinct changes in the pore current–voltage curves, such as different currents and threshold voltages for NDR, and show different dependencies on salt concentration and temperature. Thus, the procedure outlined in Fig. 1 allows the design of nanofluidic devices with tunable NDR properties. The solubility values of various weakly soluble salts are also included in Table I to provide a rough estimate under which experimental conditions precipitation and NDR can appear. For our conical nanopores, the external solution concentrations we used in each case were in the range of 1 to 100 mM.

TABLE I. Different electrolyte pairs forming weakly soluble salts (third column) that show nanoscale precipitation phenomena similar to those of Fig. 1 for distinct cations and anions. The respective bulk solution solubilities are indicated for qualitative purposes only.

Tip solution	Base solution	Precipitate	Solubility at 20 °C (g/100 ml)
RbCl	KIO_3	$RbIO_3$	2.6
CsCl		$CsIO_3$	1.96
$CaCl_2$	$NaIO_3$	$Ca(IO_3)_2$	0.24
$SrCl_2$		$Sr(IO_3)_2$	0.19
$BaCl_2$		$Ba(IO_3)_2$	0.035
$CaCl_2$	K_2SO_4	$CaSO_4$	0.26
$SrCl_2$	Na_2SO_4	$SrSO_4$	0.0132
$BaCl_2$		$BaSO_4$	2.44×10^{-4}
KCl	$LiClO_4$	$KClO_4$	1.68
RbCl	$NaClO_4$	$RbClO_4$	1.55
CsCl		$CsClO_4$	1.60
KCl	$NaIO_4$	KIO_4	0.42
RbCl		$RbIO_4$	0.648
CsCl		$CsIO_4$	2.2
LiCl	KF	LiF	0.127
$CaCl_2$		CaF_2	1.6×10^{-5}
$SrCl_2$		SrF_2	1.17×10^{-4}
$BaCl_2$		BaF_2	1.6×10^{-3}
$CaCl_2$	KCl, pH basic	$Ca(OH)_2$	0.173
$CaCl_2$	Na_2CO_3	$CaCO_3$	$1.3\ 10^{-3}$
$BaCl_2$		$BaCO_3$	0.024

In order to achieve reproducible NDR through precipitation, as a general rule, the nanopores should exhibit a high rectification ratio in KCl and a narrow tip diameter. The high asymmetry of current–voltage curves in KCl assures a high level of ionic enhancement that enables precipitation in the presence of ions creating a weakly soluble salt. High rectification also indicates a strong ionic depletion for the opposite voltage polarity that helps reset the system and clear the precipitate. A small tip opening enhances voltage-modulation of local ionic concentrations and makes the precipitate more localized.

Figure 2 shows the NDR phenomena observed with three different pore samples and five electrolyte pairs (Table I). Additional examples with more pore samples and electrolyte pairs are included in Figs. S1–S7 of the supplementary material. The pair $CaCl_2$ (tip) and $NaIO_3$ (base) results in the $Ca(IO_3)_2$ precipitate [Fig. 2(a)], while the pair $CaCl_2$ (tip) and Na_2SO_4 (base) leads to formation of the $CaSO_4$ precipitate [Fig. 2(b)], obtained with pore sample No. 1. The pair LiCl (tip) and KF (base) creates the LiF precipitate [Fig. 2(c)], measured with pore sample No. 2. Finally, the salts CsCl (tip) and $LiClO_4$ (base) give rise to the $CsClO_4$ precipitate, while KCl (tip) and $NaClO_4$ (base) result in the formation of the $KClO_4$ precipitate [Fig. 2(d)], obtained with pore sample No. 3. In all cases, the precipitate blocks the pore in the forward bias ($V > 0$), when concentrations of cations and anions are enhanced. The onset of NDR, however, occurs at distinct V_{th} and current ranges and is salt dependent. Moreover, for $CaSO_4$, LiF, $KClO_4$, and $CsClO_4$, the current switches between two states of few tens of nA and nearly zero current, respectively, achieving *on*/*off* ratios in the range 50–200. At the reverse bias voltage, the precipitate is cleared either by dissolution or electrokinetic passage, and the pore conductance is reset following a new voltage cycle. Note that even though all precipitates in Fig. 2 have similar solubility values, each pair of salts leads to distinct current–voltage characteristics that are remarkably reproducible in the successive voltage scans. The results suggest that the chemistry of the precipitate affects voltage and characteristics of precipitation-induced NDR.

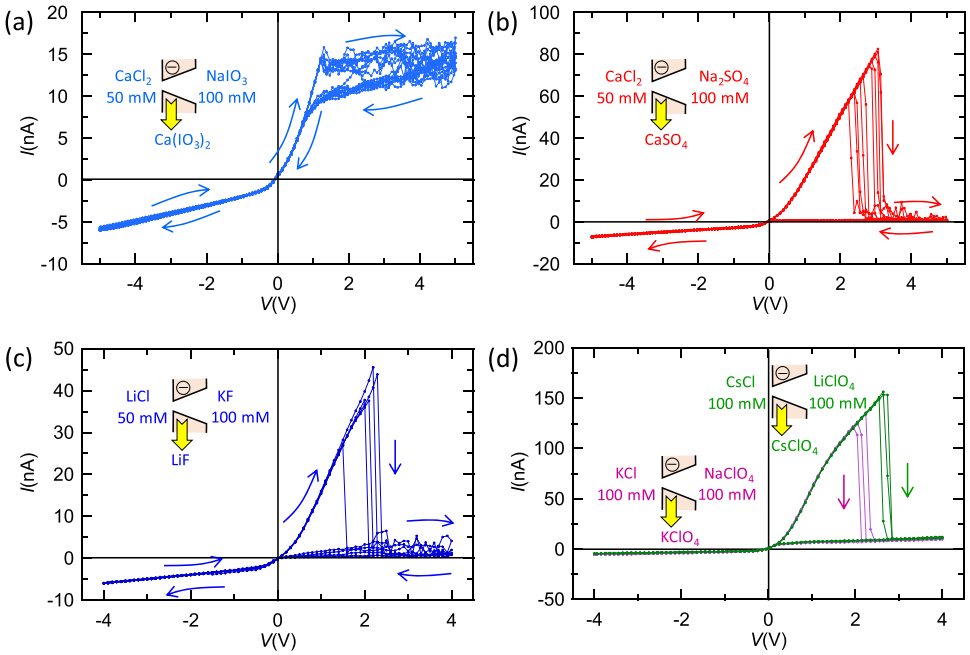

FIG. 2. NDR phenomena observed with different electrolytes and pore samples. (a) $CaCl_2$ (tip) and $NaIO_3$ (base), creating the $Ca(IO_3)_2$ precipitate, in pore sample No. 1. (b) $CaCl_2$ (tip) and Na_2SO_4 (base), leading to the $CaSO_4$ precipitate, in pore sample No. 1. (c) LiCl (tip) and KF (base), forming the LiF precipitate, in pore sample No. 2. (d) CsCl (tip) and $LiClO_4$ (base) (*green* curves), resulting in the $CsClO_4$ precipitate, and KCl (tip) and $NaClO_4$ (base) (*purple* curves), creating the $KClO_4$ precipitate, in pore sample No. 3. The precipitate formation blocks the pore at $V > 0$, while its clearing at $V < 0$ allows the regenerated pore to follow a new current rectification cycle.

Figure 3(a) shows a set of I–V curves of pairs CCl_2–$NaIO_3$ at concentrations 50–100 Mm for the divalent cations $C = Mg^{2+}$, Ca^{2+}, Sr^{2+}, and Ba^{2+}, resulting in the respective $C(IO_3)_2$ precipitate. Due to the high solubility of $Mg(IO_3)_2$, the I–V curve in the presence of magnesium ions does not show NDR. In addition, formation of $Ba(IO_3)_2$ and $Sr(IO_3)_2$ with the lowest solubility among all IO_3^- salts we studied led to a significant closure of the current in the forward bias ($V > 0$), such that negative currents became larger in magnitude than positive currents. This observation suggests that NDR with a high on/off ratio of conductance states requires reversibility of the precipitate reaction such that the system can reset before a new precipitate is formed. The reaction reversibility might be easier to achieve with salts that are more soluble. The huge differences in qualitative and quantitative behavior of nanopores in contact with different salts and precipitates suggest that solubility is a good control parameter to tune NDR. The current–time (I–t) traces in Fig. 3(b) show five different voltage cycles, illustrating the good reproducibility and stability of the NDR observed in all $C(IO_3)_2$ salts. The experiments of Fig. 3 revealed an interesting relationship between the magnitude of V_{th} and the solubility of the weakly soluble salts studied. Namely, in most cases, V_{th} is high for highly soluble salts, listed in Table I. However, this rule is not universal. In the case of two salts of similar solubility, other factors such as the shape and size of the precipitates, as well as the way they interact with the fixed charges may affect the value of V_{th}. This could be the case for the pairs KCl (tip)–$NaClO_4$ (base) to give $KClO_4$ and CsCl (tip)–$NaClO_4$ (base) to give $CsClO_4$.

In order to verify further that the NDR phenomenon and the concomitant current decrease are related to the salt precipitation, Figs. 3(c) and 3(d) show the effect of temperature on the I–V and I–t curves for the pair of salts $CaCl_2$–$NaIO_3$, respectively. Here, four different voltage cycles are shown. As the temperature increases, both the pore conductance and the magnitude of V_{th} increase, in agreement with our expectation based on the increase in the $Ca(IO_3)_2$ solubility with temperature observed in bulk solutions.

It is also known that solubility of $Ca(OH)_2$ decreases with the temperature increase, which is probed in nanopore samples No. 3 [Fig. 4(a)] and No. 4 [Fig. 4(b)]. To this end, we placed a neutral pH solution of $CaCl_2$ at the tip and basic KCl (pH = 11.7) at the pore base side, an arrangement that was expected to result in the formation of $Ca(OH)_2$ in the pore volume. Note that as the temperature increased from 20° to 70 °C, the pore conductance increased at low positive voltages, while the magnitude of V_{th} decreased. This result constitutes direct evidence of the mechanism shown in Fig. 1 based on the voltage-controlled concentrations at the pore tip and resulting precipitation that leads to NDR observed in the I–V curves.

As the next step, we investigated whether NDR depends on the type of cations that do not participate in the formation of the precipitate but are present at the base side of the pore, as shown in Fig. 5(a). As shown in Table I, two pairs of salts $CaCl_2$–ClO_3, with $C = Na^+$ and K^+, are expected to create the same $Ca(IO_3)_2$ precipitate. According to the scheme in Fig. 1(a), the pore conduction is dominated by the formation of $Ca(IO_3)_2$ for $V > 0$, and thus, the curves of the two pairs are expected to coincide, which is observed experimentally. For $V < 0$, however, the pore conduction is dominated either by the NaCl or the KCl electrolyte ions [Fig. 1(b)], and thus, the currents follow the cation diffusion coefficients. Figure 5(b) shows I–V curves recorded with the same salts as before but after changing the positions of ClO_3 (tip) and $CaCl_2$ (base) with respect to the case shown in Fig. 5(a). Now, according to the scheme of Fig. 1(c), the NaCl or the KCl electrolyte ions dictate conduction for

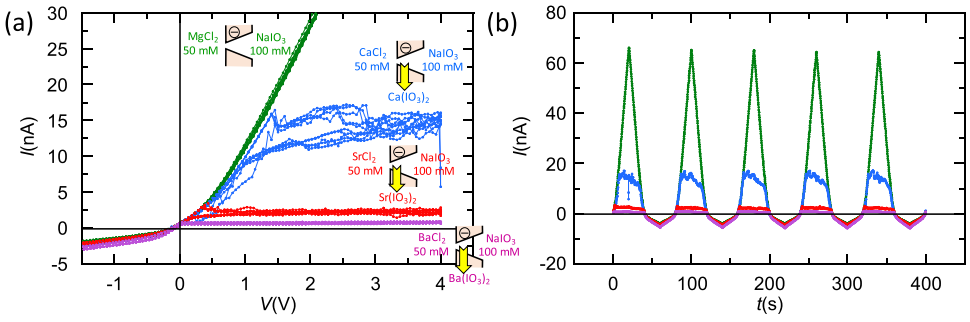

FIG. 3. (a) *I–V* curves of single nanopores in contact with pairs of salts CCl_2–$NaIO_3$, with $C = Mg^{2+}$ (*green* curve), Ca^{2+} (*blue* curve), Sr^{2+} (*red* curve), and Ba^{2+} (*purple* curve), for the respective $C(IO_3)_2$ precipitations observed at the concentrations shown (*insets*). There is a significant correlation between the magnitude of V_{th} and the solubility of the salts created in the pore, such that salts with lower solubility values tend to display NDR at smaller magnitudes of V_{th}. Note that $Mg(IO_3)_2$ is highly soluble and does not show NDR. (b) The corresponding *I–t* traces illustrate good NDR reproducibility. (c) Effect of temperature on the *I–V* curves of the pair $CaCl_2$–$NaIO_3$. Both the $Ca(IO_3)_2$ solubility and V_{th} increase with temperature. (d) Effects of temperature on the *I–t* traces under the same conditions as in (c). All experiments were conducted with pore sample No. 1.

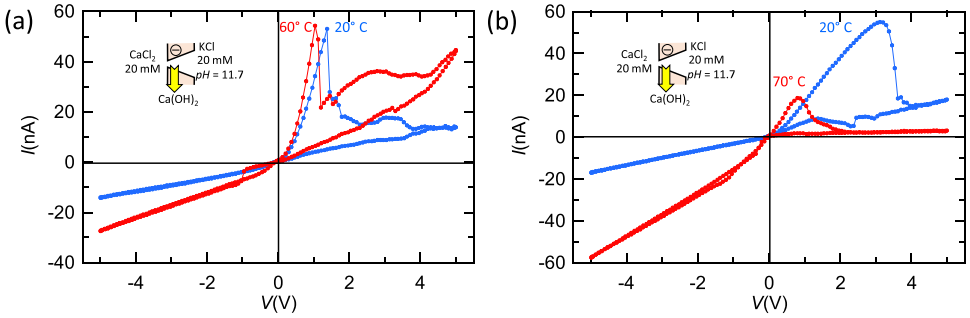

FIG. 4. Effect of temperature on the *I–V* curves of the pair $CaCl_2$ (neutral pH)–KCl (basic pH) measured in pore sample No. 3 (a) and in pore sample No. 4 (b). Contrary to the case of most pairs of salts and precipitates listed in Table I, the $Ca(OH)_2$ precipitate presents retrograde solubility, decreasing with temperature, as shown by V_{th} in both pore samples.

$V > 0$, with the electric currents following again the cation diffusion coefficients and yielding no NDR. For $V < 0$, the small, rectified currents are mainly due to the Ca^{2+} and IO_3^- ions delivered from opposite pore openings [Fig. 1(d)], and the corresponding *I–V* curves tend to coincide.

Precipitation of weakly soluble salts and resulting NDR in our system result from voltage-controlled ionic concentrations in the pore, enabled by the pore shape and surface charge. We have therefore also looked at the possibility of tuning NDR by pH of the solution that will affect the effective surface charge through the change of carboxyl group protonation. Figure 6 shows the effects of solution pH on the NDR phenomena for the salt pair $CaCl_2$–$NaIO_3$. At neutral pH [Fig. 6(a)], the pore is negatively charged, and precipitation is only observed in the case $CaCl_2$ (tip)–$NaIO_3$ (base) for $V > 0$. At pH = 3 [Fig. 6(b)], the pore is almost neutral, and the $Ca(IO_3)_2$ concentration at the pore tip is not sufficient to create precipitates. Thus, neither rectification nor NDR is observed. Finally, at pH = 2 [Fig. 6(c)], the pore is positively charged, and the rectification reverses its direction. The roles of cations and anions are interchanged with respect to the case of Fig. 1(a) such that accumulation of anions and cations occurs now for negative voltages. Thus, precipitation and NDR are only observed at $V < 0$ for the case $NaIO_3$ (tip)–$CaCl_2$ (base). At pH = 1 [Fig. 6(d)], the protons dominate conduction in the two electrolyte configurations, and no NDR is observed.

In the remaining part of this work, we focus on the $CaCl_2$–$NaIO_3$ case because of the relevant role of Ca^{2+} in multiple physico-chemical processes and the remarkable stability of V_{th} over successive cycles. A nanopore in contact with the pair $CaCl_2$ (tip)–$NaIO_3$ (base) exhibits NDR curves with stable and reproducible V_{th} values over several cycles. We propose that this property could be used for Ca^{2+} sensing over a wide concentration range. Figure 7(a) shows the effect of $CaCl_2$ concentration on the *I–V* curves for the system $CaCl_2$ (tip)–$NaIO_3$ (base). For the sake of clarity, only the data of a single cycle at voltages $V > 0$ and the concentrations of $CaCl_2$ indicated are shown. As expected, V_{th} decreases as the concentration of Ca^{2+} at the tip increases. Figure 7(b) illustrates the stability of V_{th} over ten successive cycles when KIO_3

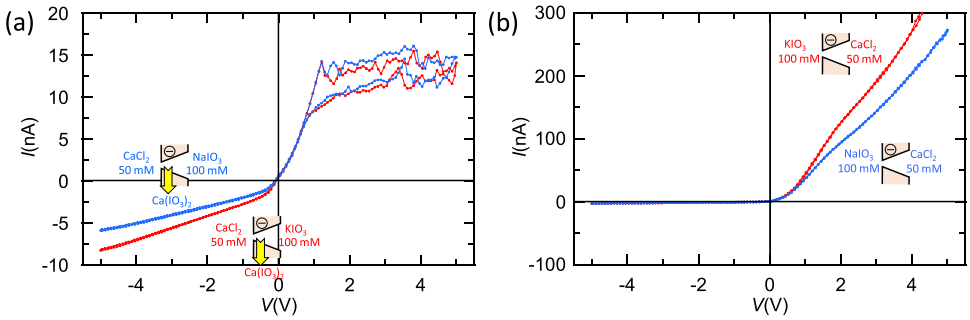

FIG. 5. (a) *I–V* curves of a single nanopore recorded for the salt pairs $CaCl_2$ (tip)–ClO_3 (base), with $C = Na^+$ (*blue* curve) and K^+ (*red* curve), at the concentrations shown (*insets*). At $V > 0$, conduction is dominated by the $Ca(IO_3)_2$ electrolyte ions, and the two curves are similar. At $V < 0$, conduction is dominated by the NaCl and KCl electrolyte ions, and the currents follow the cation diffusion coefficients. (b) *I–V* curves obtained over a single voltage cycle by changing the position of ClO_3 (tip) and $CaCl_2$ (base) electrolytes with respect to the above case. In this configuration, the NaCl and KCl electrolytes dictate ionic conduction at $V > 0$ and no NDR is obtained. On the contrary, the small, rectified currents at $V < 0$ are due to the Ca^{2+} and IO_3^- ions. All experiments were conducted with pore sample No. 1.

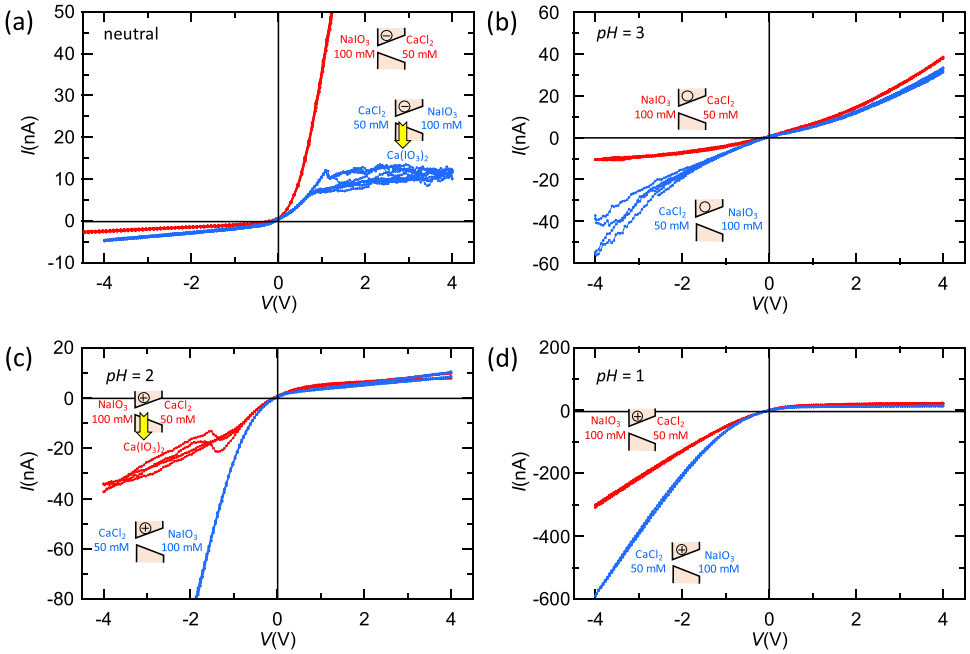

FIG. 6. Effects of the solution pH on the NDR phenomena measured over two voltage cycles. (a) Neutral pH and negative pore charge. Precipitation and NDR occur only for the system $CaCl_2$ (tip)–$NaIO_3$ (base) at $V > 0$. (b) At pH = 3, the pore walls become neutral, and consequently, neither rectification nor precipitation is observed. (c) At pH = 2, the pore becomes positively charged, and the roles of cations and anions are interchanged with respect to the case of Fig. 1(a). Precipitation and NDR occur for the system $NaIO_3$ (tip)–$CaCl_2$ (base) only at $V < 0$. (d) At pH = 1, no NDR can occur because protons dominate conduction. All experiments were conducted with pore sample No. 1.

or $NaIO_3$ is present on the base side of the pore. Figure 7(c) on the other hand, demonstrates the stability of V_{th} over ten cycles at four different concentrations of Ca^{2+} ions at the tip, with $NaIO_3$ at the base of the pore. Remarkably, the values of V_{th} become more stable as the concentration of Ca^{2+} increases, with changes lower than 0.01 V for the 1000 mM Ca^{2+} case over ten cycles. Figure 7(d) shows the calibration curve obtained for Ca^{2+} sensing with the average values of V_{th} measured over ten cycles and ten different $CaCl_2$ concentrations in the range 1–1000 mM. Further data obtained with pore sample Nos. 2 and 3 confirming the reproducibility and stability of V_{th} with pairs $CaCl_2$ (tip)–$NaIO_3$ (base) and $CaCl_2$ (tip)–KIO_3 (base) have been included in Figs. S7 and S8 of the supplementary material.

To further corroborate the results of Fig. 7, Fig. 8 demonstrates the specificity for ion sensing based on the NDR phenomena of Fig. 1. Figure 8(a) shows the *I–V* curve of a single pore in contact with the following salts: the solution mixture 10 mM $CaCl_2$ + 90 mM KCl (tip)–100 mM $NaIO_3$ (base solution). Because this electrolyte arrangement results in the low solubility salt $Ca(IO_3)_2$ and soluble salt KIO_3 at the pore tip, the *I–V* curve shows the NDR characteristics of Fig. 2(a). The precipitate formation was therefore unaffected by the addition of KCl to the tip side of the pore. When the base solution is changed to $NaClO_4$ [Fig. 8(b)], the NDR is induced by the low solubility salt $KClO_4$ formed at the pore tip, alongside the highly soluble $Ca(ClO_4)_2$; thus, the *I–V* curves obtained are similar to those of Fig. 2(d).

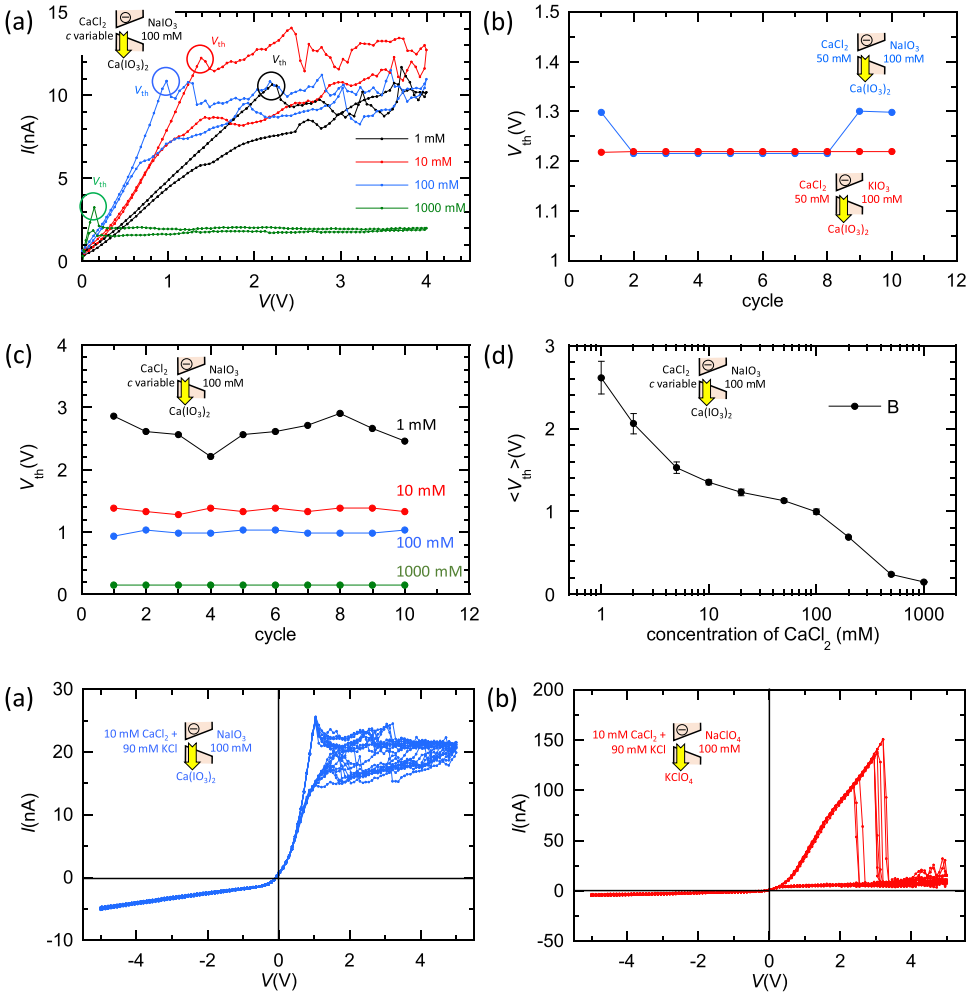

FIG. 7. (a) Effect of $CaCl_2$ concentration on the NDR phenomena for the system $CaCl_2$ (tip)–$NaIO_3$ (base) at $V > 0$ and a single voltage cycle. The threshold potential V_{th} decreases with the increase in Ca^{2+} concentration in the tip solution. (b) The stability of V_{th} over different cycles is conserved when substituting KIO_3 for $NaIO_3$ in the base solution. (c) The changes in V_{th} over ten cycles decrease with the increase in Ca^{2+} concentration. (d) The mean value $\langle V_{th} \rangle$ averaged over ten cycles as a function of $CaCl_2$ concentration allows us to define a calibration curve for Ca^{2+} sensing in the range 1–1000 mM. All experiments were conducted with pore sample No. 1.

FIG. 8. Ca^{2+} and K^+ ion sensing in the solution mixture 10 mM $CaCl_2$ + 90 mM KCl. (a) Ca^{2+} sensing with $NaIO_3$ (base solution). (b) K^+ sensing with $NaClO_4$ (base solution). Note the different electrolyte precipitations and NDR characteristics obtained by changing the base solution. All experiments were conducted with pore sample No. 1.

IV. CONCLUSION

We have described the NDR phenomena due to the nanoscale salt precipitation that occurs in a conical nanopore in contact with two highly soluble salts that react at the pore volume and create precipitates. To this end, we have designed a general procedure that leads to reproducible and tunable NDR probed through I–V curves. The tunability stems from the choice of salts and the solubility of precipitates they form. We identified pairs of salts whose precipitates cause switching of nanopore conductance with *on*/*off* current ratios in the range 50–200. In addition, we have studied the effects of pH and salt concentration on the precipitation and NDR for electrolytes with different temperature-dependent solubilities. The precipitation-based NDR phenomena are reproducible, and the threshold voltage needed for the precipitation to occur, which marks the NDR onset, shows great stability over many voltage cycles. Thus, we have proposed that the observed voltage thresholds could be used for ionic sensing. The experimental system design permits to study salt precipitation under nanoscale conditions, which should be of interest to biophysical chemistry, chemical engineering, and pharmaceutical sciences,[15,17,29,30] particularly for the case of calcium ions. This work has focused on controlling NDR probed mostly through current–voltage curves. Recording ion current time series with high time resolution and the corresponding spectral analysis, planned in future studies, will provide further insights into the fluctuations of ion transport, as previously shown in biological[31–33] and solid-state[34–36] pores.

SUPPLEMENTARY MATERIAL

The supplementary material includes additional electrolyte pairs giving precipitation and their I–V curves showing NDR phenomena.

ACKNOWLEDGMENTS

S.P., J.C., S.M., and P.R. acknowledge the support from the Conselleria d'Educació, Universitats i Ocupació (Generalitat Valenciana), Project No. CIAICO2022-247. Z.S.S. was supported by the National Science Foundation CBET-2408924. We thank Dr. Saima

Nasir and Dr. Mubarak Ali for preparing the membrane samples and Professor Wolfgang Ensinger for his assistance.

AUTHOR DECLARATIONS

Conflict of Interest

The authors have no conflicts to disclose.

Author Contributions

Patricio Ramirez: Conceptualization (lead); Investigation (equal); Methodology (equal); Resources (equal); Visualization (equal); Writing – review & editing (equal). **Sergio Portillo**: Formal analysis (equal); Investigation (equal); Methodology (equal); Writing – review & editing (equal). **Salvador Mafe**: Conceptualization (equal); Formal analysis (equal); Funding acquisition (equal); Supervision (equal); Writing – original draft (lead). **Zuzanna S. Siwy**: Conceptualization (equal); Formal analysis (equal); Investigation (equal); Methodology (equal); Writing – review & editing (equal). **Javier Cervera**: Conceptualization (equal); Formal analysis (equal); Funding acquisition (equal); Project administration (lead); Supervision (equal); Writing – review & editing (equal).

DATA AVAILABILITY

The data that support the findings of this study are available from the corresponding author upon reasonable request.

REFERENCES

[1] K. Kobashi, R. Hayakawa, T. Chikyow, and Y. Wakayama, "Negative differential resistance transistor with organic p-n heterojunction," Adv. Electron. Mater. **3**, 1700106 (2017).
[2] M. Faghih, D. Karnaushenko, Q. A. Besford, C. Becker, R. Ravishankar, D. D. Karnaushenko, G. Cuniberti, A. Fery, and O. G. Schmidt, "Membranotronics: Bioinspired nonlinear ion transport with negative differential resistance based on elastomeric membrane system," Adv. Funct. Mater. **32**, 2200233 (2022).
[3] Z. S. Siwy, M. R. Powell, E. Kalman, R. D. Astumian, and R. S. Eisenberg, "Negative incremental resistance induced by calcium in asymmetric nanopores," Nano Lett. **6**, 473 (2006).
[4] L. Luo, D. A. Holden, W.-J. Lan, and H. S. White, "Tunable negative differential electrolyte resistance in a conical nanopore in glass," ACS Nano **6**, 6507 (2012).
[5] Y. Li, G. Du, G. Mao, J. Guo, J. Zhao, R. Wu, and W. Liu, "Electrical field regulation of ion transport in polyethylene terephthalate nanochannels," ACS Appl. Mater. Interfaces **11**, 38055 (2019).
[6] Y. A. Perez Sirkin, I. Szleifer, and M. Tagliazucchi, "Voltage-triggered structural switching of polyelectrolyte-modified nanochannels," Macromolecules **53**, 2616 (2020).
[7] Q. Sheng, Y. Xie, J. Li, X. Wang, and J. Xue, "Transporting an ionic-liquid/water mixture in a conical nanochannel: A nanofluidic memristor," Chem. Commun. **53**, 6125 (2017).
[8] C.-Y. Lin, P.-H. Wong, P.-H. Wang, Z. S. Siwy, and L.-H. Yeh, "Electrodiffusioosmosis-induced negative differential resistance in pH-regulated mesopores containing purely monovalent solutions," ACS Appl. Mater. Interfaces **12**, 3198 (2020).
[9] P. Ramirez, J. J. Perez-Grau, J. Cervera, S. Nasir, M. Ali, W. Ensinger, and S. Mafe, "Negative differential resistance and threshold-switching in conical nanopores with KF solutions," Appl. Phys. Lett. **118**, 181903 (2021).
[10] J. J. Perez-Grau, P. Ramirez, V. Garcia-Morales, J. Cervera, S. Nasir, M. Ali, W. Ensinger, and S. Mafe, "Fluoride-induced negative differential resistance in nanopores: Experimental and theoretical characterization," ACS Appl. Mater. Interfaces **13**, 54447 (2021).
[11] B. Riza Putra, M. Carta, R. Malpass-Evans, N. B. McKeown, and F. Marken, "Potassium cation induced ionic diode blocking for a polymer of intrinsic microporosity|nafion 'heterojunction' on a microhole substrate," Electrochim. Acta **258**, 807 (2017).
[12] G. Laucirica, L. M. Hernández Parra, A. L. Huamani, M. F. Wagner, A. G. Albesa, M. E. Toimil-Molares, W. Marmisollé, and O. Azzaroni, "Insight into the transport of ions from salts of moderated solubility through nanochannels: Negative incremental resistance assisted by geometry," Nanoscale **16**, 12599 (2024).
[13] G. Laucirica, M. E. Toimil-Molares, W. A. Marmisollé, and O. Azzaroni, "Unlocking nanoprecipitation: A pathway to high reversibility in nanofluidic memristors," ACS Appl. Mater. Interfaces **16**, 58818 (2024).
[14] S. H. Han, S. I. Kim, M.-A. Oh, and T. D. Chung, "Iontronic analog of synaptic plasticity: Hydrogel-based ionic diode with chemical precipitation and dissolution," Proc. Natl. Acad. Sci. U. S. A. **120**, e2211442120 (2022).
[15] Z. Zhu, D. Wang, Y. Tian, and L. Jiang, "Ion/molecule transportation in nanopores and nanochannels: From critical principles to diverse functions," J. Am. Chem. Soc. **141**, 8658 (2019).
[16] T. Ma, J. M. Janot, and S. Balme, "Track-etched nanopore/membrane: From fundamental to applications," Small Methods **4**, 2000366 (2020).
[17] G. Pérez-Mitta, M. E. Toimil-Molares, C. Trautmann, W. A. Marmisollé, and O. Azzaroni, "Molecular design of solid-state nanopores: Fundamental concepts and applications," Adv. Mater. **31**, 1901483 (2019).
[18] S. Portillo, J. A. Manzanares, P. Ramirez, J. Bisquert, S. Mafe, and J. Cervera, "pH-dependent effects in nanofluidic memristors," J. Phys. Chem. Lett. **15**, 7793 (2024).
[19] Y. Hou, Y. Ling, Y. Wang, M. Wang, Y. Chen, X. Li, and X. Hou, "Learning from the brain: Bioinspired nanofluidics," J. Phys. Chem. Lett. **14**, 2891 (2023).
[20] P. Ramirez, V. Garcia-Morales, V. Gomez, M. Ali, S. Nasir, W. Ensinger, and S. Mafe, "Hybrid circuits with nanofluidic diodes and load capacitors," Phys. Rev. Appl. **7**, 064035 (2017).
[21] D. Shi, W. Wang, Y. Liang, L. Duan, G. Du, and Y. Xie, "Ultralow energy consumption Angstrom-fluidic memristor," Nano Lett. **23**, 11662 (2023).
[22] P. Robin, T. Emmerich, A. Ismail, A. Niguès, Y. You, G.-H. Nam, A. Keerthi, A. Siria, A. K. Geim, B. Radha, and L. Bocquet, "Long-term memory and synapse-like dynamics in two-dimensional nanofluidic channels," Science **379**, 161 (2023).
[23] T. Xiong, C. Li, X. He, B. Xie, J. Zong, Y. Jiang, W. Ma, F. Wu, J. Fei, P. Yu, and L. Mao, "Neuromorphic functions with a polyelectrolyte-confined fluidic memristor," Science **379**, 156 (2023).
[24] P. Ramirez, V. Gómez, J. Cervera, S. Mafe, and J. Bisquert, "Synaptical tunability of multipore nanofluidic memristors," J. Phys. Chem. Lett. **14**, 10930 (2023).
[25] J. Cervera, S. Portillo, P. Ramirez, and S. Mafe, "Modeling of memory effects in nanofluidic diodes," Phys. Fluids **36**, 047129 (2024).
[26] P. Y. Apel, Y. E. Korchev, Z. Siwy, R. Spohr, and M. Yoshida, "Diode-like single-ion track membrane prepared by electro-stopping," Nucl. Instrum. Methods Phys. Res., Sect. B **184**, 337 (2001).
[27] J. Cervera, B. Schiedt, R. Neumann, S. Mafé, and P. Ramírez, "Ionic conduction, rectification, and selectivity in single conical nanopores," J. Chem. Phys. **124**, 104706 (2006).
[28] H. S. White and A. Bund, "Ion current rectification at nanopores in glass membranes," Langmuir **24**, 2212 (2008).
[29] J. Dressman and C. Reppas, "Drug solubility: How to measure it, how to improve it," Adv. Drug Delivery Rev. **59**, 531 (2007).
[30] V. M. Aguilella, M. Queralt-Martín, M. Aguilella-Arzo, and A. Alcaraz, "Insights on the permeability of wide protein channels: Measurement and interpretation of ion selectivity," Integr. Biol. **3**, 159 (2011).
[31] S. M. Bezrukov and M. Winterhalter, "Examining noise sources at the single-molecule level: 1/f noise of an open maltoporin channel," Phys. Rev. Lett. **85**, 202 (2000).
[32] S. M. Bezrukov and J. J. Kasianowicz, "Current noise reveals protonation kinetics and number of ionizable sites in an open protein ion channel," Phys. Rev. Lett. **70**, 2352 (1993).

[33]A. Fragasso, S. Schmid, and C. Dekker, "Comparing current noise in biological and solid-state nanopores," ACS Nano **14**, 1338 (2020).
[34]K. Matsui, Y. Goto, I. Yanagi, R. Akahori, M. Fujioka, T. Ishida, T. Yokoi, T. Nakagawa, and K.-i. Takeda, "Low-frequency noise induced by cation exchange fluctuation on the wall of silicon nitride nanopore," Sci. Rep. **10**, 8662 (2020).
[35]P. Robin, M. Lizée, Q. Yang, T. Emmerich, A. Siria, and L. Bocquet, "Disentangling 1/*f* noise from confined iondynamics," Faraday Discuss. **246**, 556 (2023).
[36]R. M. M. Smeets, U. F. Keyser, N. H. Dekker, and C. Dekker, "Noise in solid-state nanopores," Proc. Natl. Acad. Sci. U. S. A. **105**, 417 (2008).